Direct calculation of the transport properties of disordered AlAs/GaAs superlattices from the electronic and phonon spectra

Lin-Wang Wang and Alex Zunger
National Renewable Energy Laboratory, Golden, Colorado 80401

Kurt A. Mäder
Centre Européen de Calcul Atomique et Moléculaire, Ecole Normale Supérieure, 69364 Lyon cedex 07, France

(Received 4 August 1995)

We have calculated from first principles the recently measured electron and hole transport of disordered AlAs/GaAs superlattices, in which the individual layer thicknesses $n,m,n',m',\ldots$ of sequence $(\mathrm{AlAs})_n(\mathrm{GaAs})_m(\mathrm{AlAs})_{n'}(\mathrm{GaAs})_{m'}\ldots$ are 1, 2, or 3, selected at random with equal probabilities. First, the near-edge electronic states are calculated using a three-dimensional pseudopotential representation for a $\sim$2000-ML cell. The results are then modeled by an effective-mass approximation, thus obtaining the electronic states in a wider energy range. All electronic states are found to be localized in the superlattice direction. Second, the phonon-assisted-hopping probabilities between different localized electronic states are calculated from first principles, including contributions of polar optical, acoustic deformation-potential, and acoustic piezoelectrical effects. Third, the master equation describing electron transport via phonon-assisted hopping is addressed using Monte Carlo simulations. The resulting transport properties versus temperature are analyzed according to dispersive transport theories, including the crossover from dispersive to equilibrium transport. A simple model for the photoluminescence process is proposed on the basis of the transport calculations. Our results agree qualitatively with recent experimental data.

I. INTRODUCTION

The introduction of intentional one-dimensional disorder in semiconductor superlattices (SL's) has been shown to have a profound impact on their electronic and optical properties:[1–5] (i) the electronic band gap is reduced significantly,[2] (ii) the photoluminescence (PL) intensity is much larger than in ordered SL's and decays more slowly with temperature,[4] and (iii) the PL intensity exhibits a strong nonexponential time dependence in a wide temperature range.[5] These striking features are of particular interest for SL's, where one or both of the components are indirect-gap materials, because the weak PL intensity that is rapidly quenched by raising temperature can be converted *via* introduction of layer randomness to strong and slowly quenched PL. Examples for such superlattice materials include AlAs/GaAs SL's (having an indirect-gap for small period ordered SL's), and AlP/GaP and Si/Ge SL's (which are indirect or pseudodirect ordered SL's for all periods).

We have recently studied[6,7] the electronic states of disordered AlAs/GaAs SL's proposed by Sasaki *et al.*[2] using accurate three-dimensional (3D) empirical pseudopotential theory. We found that all electronic states are localized in the growth direction, and that the calculated band gaps of the d-SL's agreed quantitatively with experiment. Furthermore, we showed that optical transition between localized states can be as strong as in direct-gap materials, thus explaining the enhancement of PL in the d-SL. Starting from the calculated electronic wave functions, we now proceed to study the temperature-dependent carrier dynamics of the vertical transport.

While previous studies of transport in disordered systems are based mostly on assumed models of the electronic states and hopping probabilities,[8] in the present case of one-dimensional disorder one can use realistic first principles electronic wave functions and phonon-mediated hopping probabilities. We included the electron-phonon interactions suggested to be important by previous studies on quantum well transport.[9–12]

The particular d-SL that we consider here is the one grown by Sasaki:[2] starting from an ordered SL (o-SL) $(\mathrm{AlAs})_2(\mathrm{GaAs})_2$, we replace at random two-ML-thick segments by one- or three-ML-thick segments, thus creating a disordered chain with randomly selected equal-probability layer thicknesses of $n=1,2,3$. In order to simulate the breaking of translational symmetry along the growth axis z, we have used unit cells with a total of 2000 *randomly* selected ML. For computational reason, each such "supercell" is repeated periodically. In Sec. II, we briefly discuss the electronic state wave functions, i.e., the localization of electronic states induced by disorder.[6] In Sec. III and Appendix A, we present a quantitative model of phonon-assisted hopping between the localized electronic states. The calculated hopping probabilities are used in Sec. IV to simulate the single-particle diffusion *via* a Monte Carlo solution of the master equation. The results are discussed in Sec. V and analyzed in Sec. VI, where a simple model of the PL process is proposed. Conclusions are given in Sec. VII.

II. LOCALIZED ELECTRONIC STATES

The single-particle electronic wave functions of the d-SL were calculated earlier[6] using a three-dimensional empirical pseudopotential method (EPM), with screened Ga, Al, and As pseudopotentials that were carefully fitted[13] to the band structure of bulk materials and short-period superlattices. At

0163-1829/96/53(4)/2010(10)/$06.00 © 1996 The American Physical Society

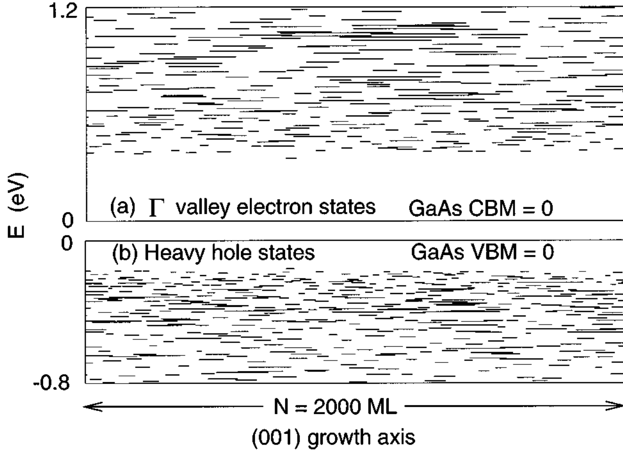

FIG. 1. Effective-mass calculated localized states of a 2000 ML AlAs/GaAs d-SL. Each line represents one eigenstate. The line length equals $2L_{\mathrm{eff}}$, where L_{eff} is the localization length, and the vertical position represent its eigenenergy. There are 285 states in the conduction band and 434 states in the valence band.

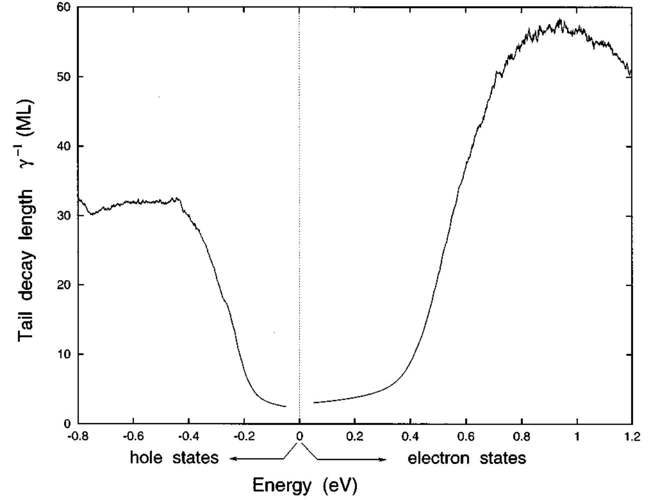

FIG. 2. Effective-mass calculated tail decay lengths γ^{-1} for the localized d-SL states. The energy zero is at the GaAs VBM for holes, and at the GaAs CBM for electrons.

this stage, we used computational supercells of up to 1000 ML total length to simulate the AlAs/GaAs d-SL. Our main findings were:[6] (i) all states are localized along the disorder z axis, (ii) the band gap is reduced by about 100 meV (redshift of PL), and (iii) the near-edge optical transition between localized states is very strong even though in the ordered SL this transition is weak, and (iv) the density of states (DOS) is nonexponential and bound from below, with a lowest possible conduction-band energy equal to that of a very long sequence of consecutive (Ga_3Al) layers. Note that the nonexponential DOS is *not* a consequence of a small (1000 atom) sample as it exists in all different randomly selected configurations of this d-SL.[7]

To facilitate fast calculations of many interelectronic matrix elements for transport calculations, a one-dimensional effective-mass approximation (EMA) was used to model the pseudopotential results.[7] In general, the 1D effective mass results were in good agreement with the 3D pseudopotential results, except for the level order of the Γ- and X-derived conduction-band edges: While the more accurate EPM shows the d-SL to be a direct-gap material (the GaAs-like, Γ-derived states are the lowest unoccupied localized states), in the EMA the AlAs-like, X-derived states are slightly below the Γ-derived ones.[7] (However, the *shape* of the EMA wave functions agrees very well with the EPM results.) We have thus ignored the X-valley states in the present study, and considered only the Γ-valley electrons. For holes, the agreement between the EPM and EMA result is quantitative.[7]

Figure 1 shows the energy vs localization range of the EMA-calculated states in a 2000 ML d-SL. Each horizontal line represents the effective length $2L_{\mathrm{eff}}$ over which the wave function is localized.[6] The vertical position of each line denotes its energy measured from the GaAs conduction-band minimum (CBM), and from the valence-band maximum (VBM), respectively. There are 285 electron and 434 hole states (not counting the twofold degeneracies of the heavy hole in the $\langle 001 \rangle$ direction) represented in Figs. 1(a) and (b), respectively. Away from the localization center, the wave functions decay exponentially with a "tail decay length" denoted by γ^{-1} and shown in Fig. 2. The information contained in Figs. 1 and 2 (energy, localization length, tail decay length) completely specifies the electronic structure parameters necessary for the transport calculation presented in the next section.

III. CALCULATING THE HOPPING PROBABILITY BETWEEN LOCALIZED STATES

Because all states of the d-SL are localized, there is no physical mobility edge, and the z direction transport can only occur *via* hopping. The hopping is induced by phonon absorption and emission. From previous work[14,15] on III-V materials, we know that at high temperature ($T > 100$ K), the polar optical phonon has the largest contribution, while at lower temperature ($T < 100$ K), the piezoelectric effect of the acoustic phonon has the largest contribution, followed by the deformation-potential effect of the acoustic phonon. We take into account all three effects for all temperatures. We ignore possible *interfacial* phonon modes, and treat the phonon system of the d-SL as the same of the pure bulk system of GaAs and AlAs with averaged frequencies.

The wave function of an electronic state $(i,\vec{k})$ can be approximated as the product of $\psi_i(z)$, the z direction localized wave function, and $\exp(-i\vec{k}\cdot\vec{r})$, a plane wave in the x,y directions (where $\vec{k}$, $\vec{r}$ are two-dimensional vectors). The energy of state $(i,\vec{k})$ can be approximated as $E(i,\vec{k}) = E_i + k^2/2m$, where E_i is the ith EMA SL eigenenergy and m is the transverse effective mass. We assume that the effective masses are equal in x and y directions, and ignore the difference in transverse mass between GaAs and AlAs; m is taken as the average value of GaAs and AlAs. In cases of nonspherical x,y effective masses, we also take an average value for m.

Our simulation of the transport (see Sec. IV) will be based on the quantum number i and not on its *substates* $(i,\vec{k})$. We, thus, need to integrate out the $\vec{k}$ degrees of freedom. Let

$P(i,j)$ denote the probability of an electron hopping from state i to state j, and let $W(i\vec{k},j\vec{k}')$ be the probability of hopping from substate $(i,\vec{k})$ to another substate $(j,\vec{k}')$. Then,

$$P(i,j)=\sum_{\vec{k}}\sum_{\vec{k}'} f_{ik}(1-f_{jk'})W(i\vec{k},j\vec{k}'), \tag{1}$$

where f_{ik} is the occupation of substate $(i,\vec{k})$. For low carrier density, nondegenerate cases, and by assuming equilibrium among the substates $(i,\vec{k})$ within each state i (reached within picoseconds due to the existence of $\vec{k}$-continuous energy levels), we have

$$f_{ik}=\frac{2\pi\beta\hbar^2}{S_{xy}m}e^{-(\hbar^2/2m)k^2\beta}, \tag{2}$$

where $\beta=1/k_BT$ and T is the temperature and S_{xy} is the x,y cross-section area of the SL. Because f_{ik} is much smaller than one (nondegenerate case), we can change Eq. (1) to

$$P(i,j)=\sum_{\vec{k}}\sum_{\vec{k}'} f_{ik}W(i\vec{k},j\vec{k}'). \tag{3}$$

$W(i\vec{k},j\vec{k}')$ can be calculated by the Fermi golden rule:

$$W(i\vec{k},j\vec{k}')=\frac{2\pi}{\hbar}\sum_{\mathbf{q}} |C(q)|^2\langle i\vec{k}|\exp(i(\mathbf{q}\cdot\mathbf{r}))|j\vec{k}'\rangle^2 \times\{N_q\delta[E(i,\vec{k})-E(j,\vec{k}')+\hbar\omega_q] +(1+N_q)\delta[E(i,\vec{k})-E(j,\vec{k}')-\hbar\omega_q]\}, \tag{4}$$

where $\mathbf{q}$ is the three-dimensional phonon wave vector, ω_q is the phonon frequency for $\mathbf{q}$, $C(q)$ is the electron-phonon coupling function, $N_q=1/[\exp(\hbar\omega_q\beta)-1]$ is the number of phonons at $\mathbf{q}$, and $|i\vec{k}\rangle$, $|j\vec{k}'\rangle$ are the electronic wave functions for states $(i,\vec{k})$ and $(j,\vec{k}')$. The electron-phonon coupling function $|C(q)|^2$ for the optical-phonon polar effect (OPP), the acoustic-phonon piezoelectric effect (APP), and the acoustic-phonon deformation-potential effect (APD) in zinc-blende structure are[16–21]

$$|C(q)|^2_{\mathrm{OPP}}=\frac{2\pi e^2}{\Omega}\left(\frac{1}{\epsilon_\infty}-\frac{1}{\epsilon_0}\right)\frac{\hbar\omega_q}{q^2}, \tag{5}$$

$$|C(q)|^2_{\mathrm{APP}}=\frac{8\pi^2e^2\hbar P^2}{\Omega\epsilon_\infty^2\rho}\frac{K_h^2}{\omega_q}, \tag{6}$$

$$|C(q)|^2_{\mathrm{APD}}=\frac{C_1^2\hbar}{2\Omega\rho C_s}q. \tag{7}$$

Here, e is the electron charge, Ω is the total volume of the system, ϵ_∞ is the electronic dielectric constant, ϵ_0 is the total (including ionic screening) dielectric constant, ρ is the density of the material, P is the piezoelectric constant ($P/2=e_{123}=e_{14}$), C_1 is deformation potential, C_s is the acoustic-phonon speed, and, finally, $K_h\equiv\hat{q}_1\hat{p}_2\hat{p}_3+\hat{q}_2\hat{p}_1\hat{p}_3+\hat{q}_3\hat{p}_1\hat{p}_2$, where $\hat{q}$, $\hat{p}$ are the unit vectors of $\mathbf{q}$ and polarization, respectively. For optical-phonon polar and acoustic-phonon deformation potential effects, we have considered in Eqs. (5) and (6) only the longitudinal mode, which has large electron-phonon coupling. For acoustic-phonon piezoelectric effect, we have considered all polarization modes. For optical phonons, we can approximate ω_q as a constant ω_0. For acoustic phonons, we can approximate ω_q as C_sq.

Substituting Eqs. (4)–(7) into Eq. (3) and carrying out analytically[22] the summation $\Sigma_{\vec{k}}\Sigma_{\vec{k}'}$, we find the analytical formulas for $P(i,j)$ as a function of the energies, positions, localization lengths, and decay lengths of state i and j. $P(i,j)$ is also a function of temperature T. The final formulas for $P(i,j)$ due to OPP, APP, and APD are given in Appendix A.

IV. MONTE CARLO SIMULATIONS

Once $P(i,j)$ is obtained at a given temperature from Eqs. (A1), (A8) and (A10) of Appendix A, Monte Carlo simulation can be performed to solve the master equation describing the population and depopulation of level i:

$$\frac{d}{dt}N_i=-N_i\sum_{j\neq i}P(i,j)+\sum_{j\neq i}N_jP(j,i), \tag{8}$$

where N_i is the occupation number of electron (or hole) in state i. The Monte Carlo method is used to simulate the random trajectory of a single electron (or hole). We study the dilute carrier limit, thus ignoring possible Coulomb interactions between electrons (or between holes). If the electron (hole) is at a given state i, then $P_i=\Sigma_{j\neq i}P(i,j)$ is the rate of hopping to other states. If R is a uniformly distributed random number between 0 and 1, then $t=-\ln(R)/P_i$ can be used as the time for the electron (hole) to have a hopping event. Using another random number R_1, one can determine to which state j the electron (hole) will hop given their probability $P(i,j)$ [this selection process from N_{stat} states can be performed in $\log_2(N_{\mathrm{stat}})$ operations, using a tree data structure]. Repeating this process, we obtain the real-space trajectory of this carrier, allowing one to watch how the electron (hole) hops from one state to another and to measure the distance traveled by the carrier. To obtain statistically averaged results, we have repeated the process with different starting states and random number sequences, and have averaged the electron's (hole's) energy $E(t)$, and the diffusion distance squared $d^2(t)$. Typically, we repeat the process 1000 times, letting each time the electron (hole) have five million hopping events. This takes a few hours of CPU time on a RS/6000 IBM workstation model 590.

V. RESULTS

Figures 3 and 4 show the energy $E(t)$ and diffusion distance squared $\bar{d}^2(t)$ curves, respectively, for electrons and holes at different temperatures. Each curve is an average of 1000 trajectories, with starting states *uniformly* distributed among the N_{stat} states shown in Fig. 1. Thus, the average $t=0$ energy is given by the centroid of Fig. 1: about CBM $+0.7$ eV for electrons and VBM-0.4 eV for holes.[23] In averaging $E(t)$ and in all of the following discussions, we use only the 1D EMA energy E_i, while the transverse kinetic energy $k_{xy}^2/2m=k_BT$ is not included (this constant can, how-

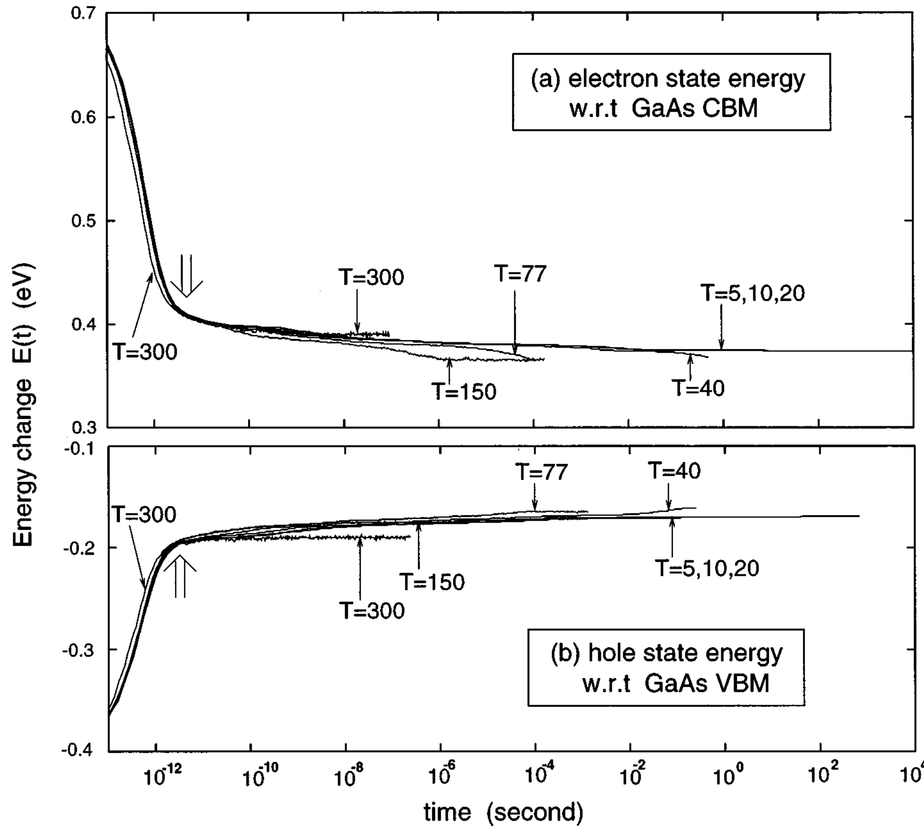

FIG. 3. Energy decay caused by phonon-assisted hopping. Each curve is an averaged result of 1000 electron or hole trajectories. The large arrows around 10^{-12} sec indicate the end of the initial fast relaxation regime.

ever, be added back trivially if needed). Figures 3 and 4 suggest the following observations.

(i) Comparison of the distances traveled by electrons and holes (at $T>77$ K and $t>10^{-10}$ sec) in Fig. 4(a) and Fig. 4(b), respectively, shows that the hole is more mobile than the electron. This reflects the larger hole density of states in the system.

(ii) Inspection of the low T curves shows that there is a characteristic baseline $T\rightarrow 0$ curve both for the $E(t)$ and $\bar{d}^2(t)$ functions. These curves reflect the result of downhill hopping (i.e., i hops to j when $E_i>E_j$ even if $T\rightarrow 0$). At short times, the curves for all temperatures follow this baseline curve.

(iii) For finite temperature T, the $E(t)$ and $\bar{d}^2(t)$ curves deviate from their baseline curves only after a critical time t_c. This indicates that uphill hopping with phonon absorption takes place for $t>t_c$.

(iv) For $T=300{,}150$ K (for electrons) and $T=300{,}150{,}77$ K (for holes), the carriers have reached equilibrium within our simulation time. This is indicated by the plateau in the $E(t)$ curves of Fig. 3 and by $\bar{d}^2(t)=2\,D(T)t$ being a straight line in Fig. 4, where $D(T)$ is the equilibrium diffusion constant. For the other temperatures considered here, equilibrium is not reached even after one second. [If the system were in equilibrium at $T=5{,}10{,}20{,}40$ K, then according to the $\{E_i\}$ spectrum of Fig. 1, more than 90% of the electron and hole occupation would have been condensed in the overall lowest energy level of the 2000 ML system.]

(v) The electron equilibrium diffusion constants $D(T)$ at $T=300{,}150$ K are calculated to be 3.7×10^{13} and 3.7×10^{11} ML^2/sec, respectively. The hole equilibrium diffusion constants at $T=300{,}150{,}77$ K are 9.1×10^{13}, 2.2×10^{12}, 5.3×10^{9} ML^2/sec, respectively. The temperature dependence of $D(T)$ is activated with $D(T)=D_0\exp(-E_0/k_BT)$, with $E_0=110{,}90$ meV for electrons and holes, respectively. Notice that this formula does not imply that we have a *physical* mobility edge. A variable range hopping model with tail states density $\sim(E-E_A)^n$ also yields[24] an almost exponentially decreasing diffusion constant vs $1/T$. A more recent work[25] using exponential tail density of states and tail state hopping also obtained an exponential decay $D(T)$ with $1/T$. (Additional discussion of this is provided in Sec. VI C.)

(vi) Diffusion constants for o-SL's are significantly larger than those of d-SL. [As we will see in Sec. VI D, this could explain the weaker temperature dependence of the PL of d-SL's relative to o-SL's.] This is seen as follows: The calculated hopping model electron diffusion constants for *ordered* $(\mathrm{GaAs})_7(\mathrm{AlAs})_7$ superlattices[26] at $T=300{,}150{,}100$ K are 4.6×10^{14}, 1.3×10^{14}, and 3.8×10^{13} ML^2/sec from Ref. 11. For $T=300$ K, these values for the ordered 7×7 SL are already an order of magnitude larger than our values for the disordered superlattice with an average 2×2 period. The value of $D(T)$ for 2×2 *ordered* superlattices must be even larger than the 7×7 results.[11] Furthermore, for 2×2 ordered SL, the localized-state hopping model may no longer hold, and the continuous-energy miniband scattering model might be more relevant.[12] If that is the case, then the diffusion constant of the 2×2 o-SL could be one or two orders of magnitude *larger* than the values from Ref. 11 for the 7×7 o-SL. Furthermore, the diffusion constant for the ordered SL drops much slower with temperature than the d-SL results.[11]

(vii) Within the first few picoseconds (see wide vertical

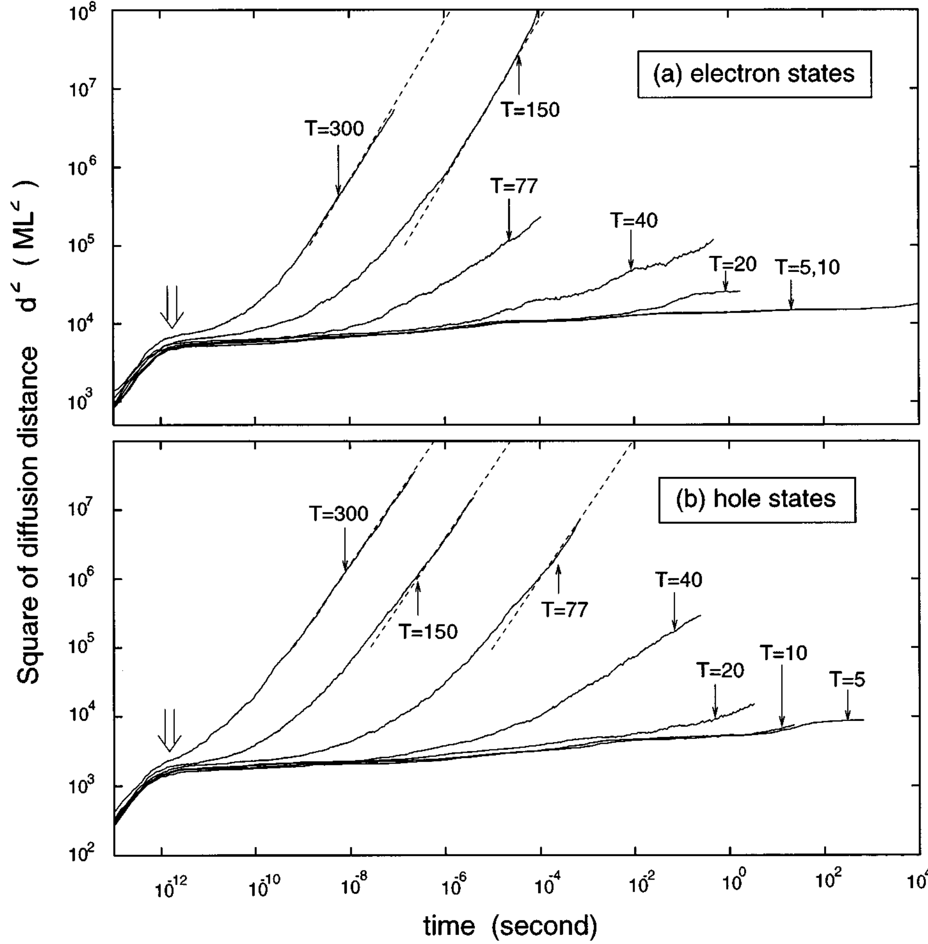

FIG. 4. Diffusion distance squared as a function of time. Each curve is an averaged result of 1000 electron (hole) trajectories. The dashed lines with slope one are the fits for equilibrium diffusion formula $d^2(t)=2D(T)t$. The large arrows around 10^{-12} sec indicate the end of the initial fast relaxation regime.

arrows in Figs. 3 and 4), the electron and hole lose energy very quickly (Fig. 3). This is the time scale characteristic of optical phonons. After the first few picoseconds, the energy drops much slower. At the end of these few picoseconds, the electron (hole) has moved an averaged distance of 77 (42) ML. This distance is larger for electrons than holes, because the electron has a smaller density of state, thus it has to find more distant states to hop to. Note that 77 (42) ML are comparable to the effective localization length of the electronic states (Fig. 1). After this initial stage, the electron and hole are trapped in local energy minima and thus move much slower.

(viii) In the typical range of time resolved PL experiments[5] (nano to microseconds), the systems below $T=300$ K have not yet reached their equilibria. For $T=150,77,40$ K, the diffusion curves of Fig. 4 already deviate from the $T=0$ baseline curve. Thus, the carriers are experiencing *dispersive* transport. This will be analyzed in more detail in the next section.

VI. ANALYSIS OF THE TRANSPORT RESULTS AND A SIMPLE MODEL FOR PHOTOLUMINESCENCE

As noted above, in the range of nano to microseconds, the d-SL at most temperatures is going through a dispersive diffusion process. A general way to describe such a system is to define a "time-dependent diffusion constant" $D(t)$.[27,28] In our case, it can be calculated as

$$D(t)=\frac{1}{2}\frac{d}{dt}\bar{d}^2(t), \tag{9}$$

where $D(t)$ is a function of the distribution of electrons (holes) at time t. Thus, roughly speaking, $D(t)$ is a function of the average energy $E(t)$. The $D(t)$'s calculated by Eq. (9) are shown in Fig. 5. We see from Fig. 5 that (i) at low temperatures $T=5,10$ K, $D(t)\propto 1/t$; (ii) for other temperatures, when $D(t)$ deviates from the $1/t$ curve, it can be described by a straight line in the log-log plot, thus $D(t)\propto 1/t^{1-\beta}$, with $0<\beta<1$; (iii) for high temperatures $T=300,150,77$ K, after equilibrium is reached, $D(t)$ is a constant. So, in general, the $D(t)$ curve for a given temperature can be represented by three straight lines in the log-log plot of Fig. 5. These are shown as dashed lines in Fig. 5. We now discuss these regimes and a simple model for the PL process.

A. The 1/*t* regime

In the $1/t$ regime, the diffusion process is purely downhill (Fig. 3), so the $1/t$ scaling of $D(t)$ can be explained as follows.[29,30] Define $D'(E)$ as a diffusion constant for an electron at energy level E. $D'(E)$ also determines a characteristic time $\tau(E)\propto 1/D'(E)$ within which the electron can diffuse away (or have a hopping event). $D'(E)$ drops rapidly with decreasing E. Thus, at time t, the electrons with $\tau(E)<t$ have already hopped to a lower energy state. Thus,

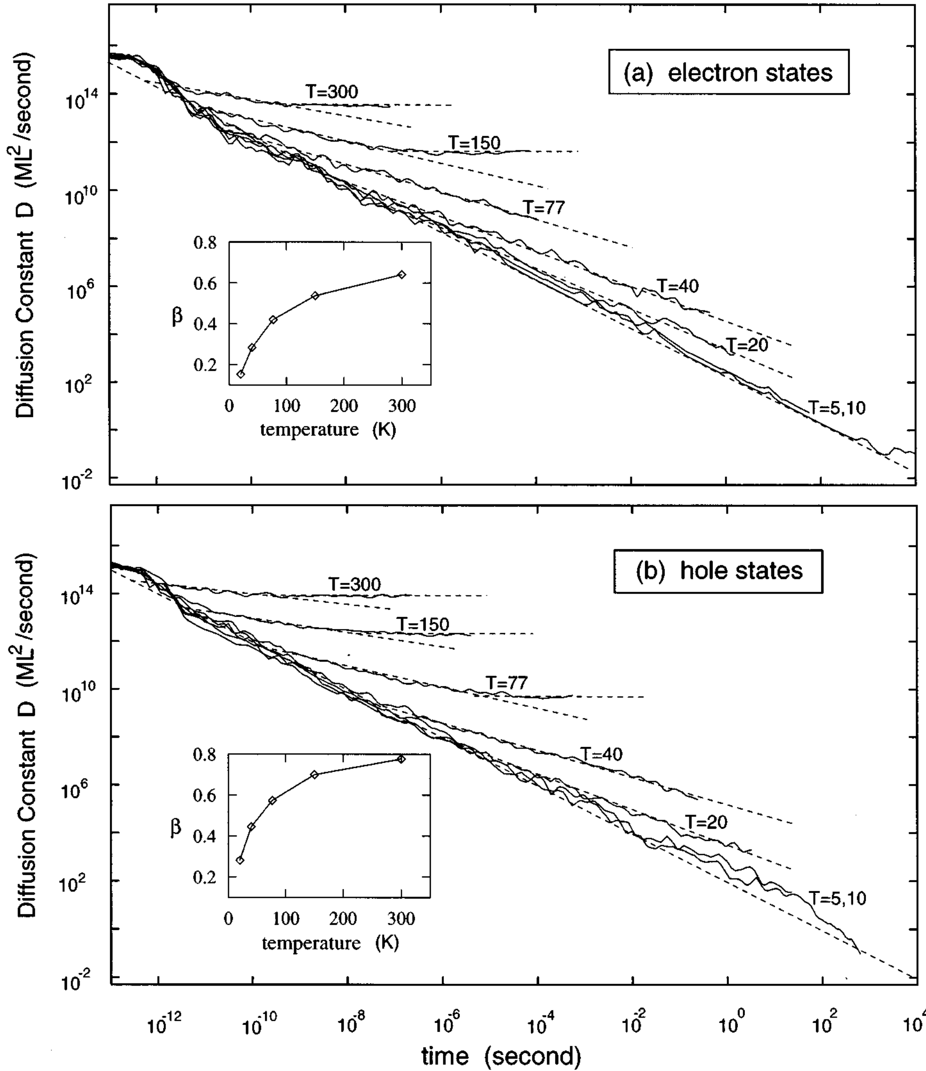

FIG. 5. Time-dependent diffusion constant $D(t)$ as calculated from Eq. (9). The dashed straight lines indicate the three different regimes in the transport as discussed in the text. The lowest dashed lines have slopes equal -1, thus $D(t)\propto 1/t$. The intermediate dashed lines have slopes larger than -1, thus $D(t) \propto 1/t^{1-\beta}$. The β's are plotted in the insets.

$\tau(E_{\rm cut})=t$ determines a cutoff energy $E_{\rm cut}$ in the electron energy distribution, above which there is no electron occupation. The total diffusion constant $D(t)$ is dominated by a small fraction of the electrons at the highest energy. Thus, $D(t)\simeq D'(E_{\rm cut})$. But $t=\tau(E_{\rm cut})\propto 1/D'(E_{\rm cut})$, so $D(t)\propto 1/t$. This argument can be applied only to low temperatures when all the hopping events are purely downhill.

B. The $1/t^{1-\beta}$ regime and the possibility of continuous-time random walks

When $D(t)$ deviates from the $1/t$ curve, it can be described by $1/t^{1-\beta}$. Such scaling is often discussed in terms of continuous-time random walks (CTRW).[31] In the CTRW model, a hopping probability distribution function $\psi(t_1)\sim t_1^{-(1+\beta)}$ is assumed and a time-of-flight experimental current $I(t)\propto t^{-(1-\beta)}$ is obtained. Physically, $I(t)$ is proportional to $D(t)$ through a constant factor. It would thus appear that the CTRW can be used to describe our results. There are a few reasons to think otherwise.

(i) In the CTRW model, $\psi(t_1)$ describes the probability distribution of the *next* hopping after a given hopping event (t_1 is measured from the absolute time t of the current hopping event). The average hopping distance is a constant d, independent of how many times the electron has hopped and when [i.e, at what t_1 in $\psi(t_1)$] the hopping occurred. This appears inconsistent with the electron transport process that we find here. In our case, the later the hopping happens in $\psi(t_1)$, the longer the hopping distance d is. Furthermore, $\psi(t_1)$ is a function of the number of times the electron has already hopped. Thus, in our case, $\psi(t_1)$ seems to depend on the *absolute* time t of the current hopping event. Apparently, for larger t, the $\psi(t_1)$ has larger weight at larger t_1. Another way to look at this is to define a *time-dependent* transport energy E_t (see below) around which most of the hopping events occur. Thus the jumping distance d, which depends on E_t, is also time dependent. One can apply CTRW on fractals.[32] But in that simple model (a) the temporal effect and spatial effect are separable and uncorrelated, (b) there is no correlation between the time t of the current hopping event and the hopping distribution $\psi(t_1)$ of the next hopping event. So, we conclude that the uncorrelated CTRW model cannot be used to describe our process, although the final results are the same.

(ii) The value of β is shown in the insets of Fig. 5 as a function of temperature. Note that it cannot be described by

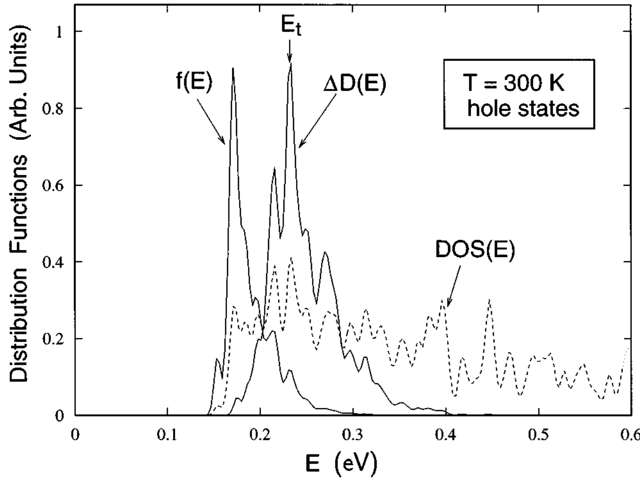

FIG. 6. The energy-resolved diffusion constants $\Delta D(E)$, the hole distribution function $f(E)$, and the density of states DOS(E). $\Delta D(E)dE$ is the contribution to the diffusion constant from energy range E to $E+dE$. See text for its calculation. $f(E)=$ DOS$(E)\exp(-E/k_BT)$. The E_t is the transport energy used in some theoretical models. (Refs. 25, 30, 33, and 34). There is a 5 meV Gaussian broadening for each curve.

T/T_0, which is a CTRW result of a multiple trapping model with an exponential density of state tail $\exp(-E/k_BT_0)$ below a physical mobility edge.[31]

Finally, (iii) in the CTRW $\psi(t_1)\sim t^{-(1+\beta)}$ model, the system reaches equilibrium only at $t\rightarrow\infty$ for exponentially decaying, unbound DOS, thus $D(t)$ will follow the $1/t^{1-\beta}$ scaling forever (in the exponential density of state tail model, for $T<T_0$, the equilibrium state corresponds to an energy distribution infinitely deep which will take an infinitely long time to reach). In reality, of course, given long enough time the system will reach equilibrium [see Sec. V items (iv) and (v)]. Thus, the $D(t)\propto 1/t^{1-\beta}$ scaling will give way to a constant (horizontal line). This happens in our simulation at $T=300,150$ K for electrons and at $T=300,150,77$ K for holes. Based on the above arguments, we conclude that one cannot use the $D(t)\propto 1/t^{1-\beta}$ scaling to justify the validity of the CTRW.

C. Equilibrium transport and the possibility of effective mobility edge

As discussed in item (v) of Sec. V, the equilibrium diffusion constants at different temperatures obey the activation formula $\exp(-E_0/k_BT)$, although there is no physical mobility edge in our system. Nevertheless, there are theories which employ the concept of *effective* mobility edge.[33,25,30,34] The essence of these theories is that the carriers need to hop to some higher energy levels in order to make subsequently more efficient hops around those high energy levels. To check such a concept, we have plotted in Fig. 6 the energy resolved diffusion constant $\Delta D(E)$ (the diffusion contribution around energy E) for holes at $T=300$ K. The integral $\int\Delta D(E)dE$ equals the total diffusion constant D. Numerically, $\Delta D(E)$ is calculated by averaging the square of the hopping distance [i.e, $(z_i-z_j)^2$] of each hopping event $E_i\rightarrow E_j$, where $\max(E_i,E_j)$ falls into the interval $[E,E+dE]$. The average is carried out after the system has reached its equilibrium. Also plotted in Fig. 6 are the hole distribution function $f(E)$ at equilibrium and the hole density of states (DOS) of the d-SL. The $\Delta D(E)$ is a rather broad function with a larger than 0.1 eV range. The maximum of $\Delta D(E)$ is often called[33,25] transport energy E_t and is sometimes regarded as an effective mobility edge.[30,34] However, we want to point out that this effective mobility edge is rather different from the real physical mobility edge of the original multiple trapping model,[35,36] because here the contribution to the diffusion comes from a rather broad range, both below and above E_t. Unlike the common theories,[33,25,30,34] which assume an exponential DOS tail $\exp(-E/k_BT_0)$, our DOS(E) around E_t does not follow such exponential form as evident from Fig. 6. Thus, while in the common theories, $f(E)=$ DOS$(E)\exp(E/k_BT)$ is exponentially increasing into the band gap region ($T<T_0$), our $f(E)$ has a peak only 60 meV below E_t and the conduction-band DOS has a lower bound cutoff. Furthermore, our $\gamma^{-1}(E)$ depends on E. Thus, a-Si theories do not directly apply to our case and more studies are needed to see how useful the concept of the effective mobility edge is in our case. A simple model which assumes tail state hopping with an exponential DOS and a constant localization decay length γ^{-1} yields[25] an activation formula $\exp(-k_BT_0/k_BT)$ for the diffusion constant D in one dimension, which seems in agreement with our results. Furthermore, as mentioned in Sec. V, item (v), models with a $\sim(E-E_A)^n$ localized band tail also yield approximately $\exp(-E_0'/k_BT)$ results.[24] So the $D(T)\sim\exp(-E_0/k_BT)$ is a very general result and can be obtained from many different situations; it does not imply an exponential DOS and multiple trapping.

D. A simple model for the PL process

Given the above transport results, we can construct a simple model for the photoluminescence process in d-SL's. While more detailed results should be obtained by direct numerical simulations (especially taking into account the effects of Coulomb interactions and the correct *radiative* transition matrix elements), here, we merely use a simple model to judge whether the PL process can be explained by considering the vertical transport alone, i.e, ignoring the details of the xy lateral transport.

We consider a geminate process. Let $I(t)$ denote the carrier density. $I(t)$ decays both because of radiative and nonradiative effects. The radiative decay is described here by a single decay time τ_a. For the nonradiative decay, it is assumed that the electron and hole will annihilated by nonradiative centers as they diffuse away from their current positions. Thus, the nonradiative channel is proportional to the diffusion constant $D(t)$ for both electrons and holes. Thus, we have

$$\frac{dI(t)}{dt}=-\alpha[D_{\rm el}(t)+D_{\rm hole}(t)]I(t)-\frac{1}{\tau_a}I(t), \qquad (10)$$

where we assume that α and τ_a are time and temperature-independent constants. The PL intensity is proportional to $I(t)$ with a prefactor $1/\tau_a$. Integrating Eq. (10), we have

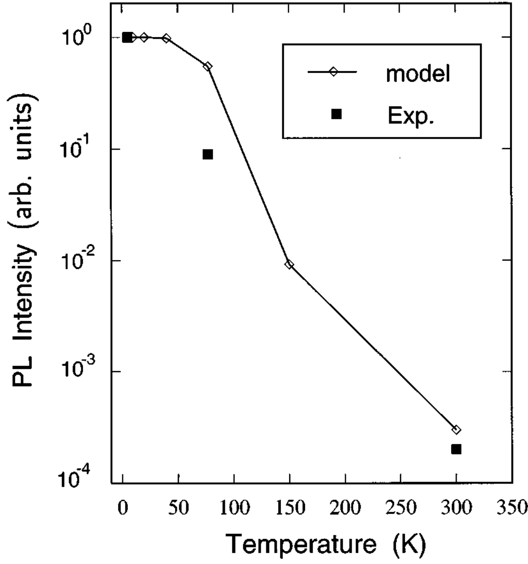

FIG. 7. The comparison of PL intensity between experimental data (Ref. 4) and our simple model results. The $T=0$ points are both normalized to one.

$$I(t)=I_0\exp\left[-\alpha\int_0^t[D_{\mathrm{el}}(t)+D_{\mathrm{hole}}(t)]dt-t/\tau_a\right]$$

$$=I_0\exp\left[-\frac{\alpha}{2}[\bar{d}^2_{\mathrm{el}}(t)+\bar{d}^2_{\mathrm{hole}}(t)]-t/\tau_a\right]. \quad (11)$$

Note that in the exponential, only one term dominates at a given time range. At the experimental time range of nanoseconds to microseconds, for T less than 300 K, the $D_{\mathrm{el}}(t)$ and $D_{\mathrm{hole}}(t)$ are described by $1/t^{1-\beta}$, thus $\bar{d}^2_{\mathrm{el}}(t)$ and $\bar{d}^2_{\mathrm{hole}}(t)$ scale as t^{β}. Thus, within this time range, the PL intensity is a stretched exponential. This agrees with the experimental results.[5] On the other hand, for higher T ($T=300$ K), $D_{\mathrm{el}}(t)$ and $D_{\mathrm{hole}}(t)$ are constants, thus the PL decays as a single exponential. This also agrees with experimental results.[5] To determine α, we required Eq. (11) to give the experimental[5] exponential decay time of 350 ps for[37] $T=300$ K. This gives $\alpha=2.2\times10^{-5}$ ML^{-2}. Assuming $\tau_a=1$ μs, we can then obtain the total PL intensity $1/\tau_a\int_0^\infty I(t)dt$ as a function of temperature T. The results are shown in Fig. 7, and compare well with experimental results.[4] In our simple model the PL process is dominated by the radiative decay itself at low temperatures ($T=5,10,20$ K). In these cases, the nonradiative channel does not play a very important role. At higher temperatures, especially for $T=300$ K, the nonradiative decay dominates the PL process [i.e, the decay of $I(t)$]. The slower drop of PL intensity with increasing temperature compared with o-SL results[4] is probably a consequence of a one or two order of magnitude smaller $D(T)$ in d-SL compared with the value in o-SL at $T=300$ K [Sec. V, item (vi)]. A more detailed comparison has to await direct PL process simulations. They might reveal whether τ_a and α are functions of t and T. Nevertheless, the overall comparison of our simple model with the experimental results is very good. *This probably means that the vertical transport is sufficient to explain the PL process.*

Finally, our vertical transport results might shed some light on the explanation of a recent PL thermal-quenching experiment.[38] Especially, the bending of the d-SL curve in Fig. 4 of Ref. 38 around $T=120$ K might correspond to the start of deviation of the $\bar{d}^2(t)$ curve from the $T=0$ baseline curve within the experimental time range.

VII. CONCLUSIONS

Starting from a realistic description of the electronic structure of disordered AlAs/GaAs SL's, we have simulated from first principles the vertical transport in the d-SL, due to phonon-assisted hopping. The lateral degrees of freedom were integrated out analytically, and the hopping probabilities between localized states along the z direction were calculated numerically, using effective mass wave functions and GaAs/AlAs material parameters pertinent to electron-phonon interaction as sole input. The hopping probabilities were then used in a Monte Carlo simulation of carrier diffusion.

We have identified the following time and temperature regimes of vertical transport.

(i) At very short times (~picoseconds), hopping is mostly downhill, and independent of temperature. At very low temperature ($T\lesssim10$ K), downhill hopping (i.e., phonon emission) continues to be the dominant process, and the diffusion "constant" behaves as $D(t)\propto1/t$. The carriers will eventually "freeze" in the lowest energy positions, and will be unlikely to escape.

(ii) At high temperature ($T\gtrsim300$ K), the carriers reach equilibrium within about a nanosecond, and the transport is then described by a standard diffusion law.

(iii) At intermediate temperatures ($T\gtrsim150$ K for electrons, and $T\gtrsim77$ K for holes, the carriers reach equilibrium after nano to microseconds. In the equilibrium regime, the diffusion constant behaves as $D(T)\propto\exp(-E_0/k_BT)$. However, E_0 is *not an activation energy to a mobility edge*, since in the quasi-one-dimensional d-SL *all states* are localized.

(iv) Before reaching equilibrium, the carriers experience dispersive transport. The diffusion "constant" is time dependent as $D(t)\propto1/t^{1-\beta}$. For intermediate temperatures, dispersive transport occurs within the experimental time span (nano to microseconds) of time-dependent PL experiments.[5] Using a simple model of geminate photoluminescence, we have shown that such a power law $D(t)$ leads to a stretched-exponential quenching of the PL intensity $I(t)$, in agreement with experiment.[5]

We have pointed out some important differences between the present results and previous models, such as continuous-time random walk, and the multiple trapping model (with a physical mobility edge), even though similar scaling laws are obtained. We also discussed the usefulness of the effective mobility edge concept in our system. Finally, our simple model of the PL process demonstrates that the PL process of the d-SL is likely explainable by the vertical transports alone, ignoring the xy direction diffusions.

ACKNOWLEDGMENTS

The authors like to thank Dr. D. Arent and Dr. H. Branz for many helpful discussions and Professor M. Kemp for very thoughtful comments on this manuscript. This work was

supported by the office of Energy Research, Materials Science Division, U.S. Department of Energy, under Grant No. DE-AC02-83CH10093.

APPENDIX A: THE FORMULAS FOR $P(i,j)$

For the *optical-phonon polar* effect:

$$P_{\rm OPP}(i,j)=f_{\rm OPP}\int_0^{q_{\max}}[N_0 e^{\lambda_+}f_g(x_+)+(N_0+1)e^{\lambda_-}f_g(x_-)]I_{ij}^2(q_z)\frac{1}{q_z}dq_z, \quad \text{(A1)}$$

where

$$f_{\rm OPP}=\frac{\omega_0 e^2}{\hbar}\left(\frac{\pi m\beta}{2}\right)^{1/2}\left(\frac{1}{\epsilon_\infty}-\frac{1}{\epsilon_0}\right), \quad \text{(A2)}$$

$$\lambda_\pm=\frac{\beta}{2}(\Delta E_\pm-|\Delta E_\pm|), \quad \text{(A3)}$$

and

$$\Delta E_\pm=E_i-E_j\pm\hbar\omega_q, \quad \text{(A4)}$$

and

$$x_\pm=\left(\frac{\beta\hbar^2}{2m}\right)^{1/2}\left(\frac{q_z}{2}+\frac{m|\Delta E_\pm|}{\hbar^2 q_z}\right), \quad \text{(A5)}$$

and

$$f_g(x)=\frac{2}{\sqrt{\pi}}e^{x^2}\int_x^\infty e^{-t^2}dt. \quad \text{(A6)}$$

$N_0=1/[\exp(\hbar\omega_0\beta)-1]$ in Eq. (A1) and $\omega_q=\omega_0$ in Eq. (A4) for the optical phonon. $q_{\max}$ in Eq. (A1) is determined by the boundary of the phonon Brillouin zone. Finally, $I_{ij}(q_z)$ is defined as

$$I_{ij}(q_z)=\int \psi_i(z)\psi_j^*(z)e^{iq_z z}dz, \quad \text{(A7)}$$

where $\psi_i(z)$ and $\psi_j(z)$ are normalized, one-dimensional localized wave functions for states i and j.

For the *acoustic-phonon deformation-potential* effect:

$$P_{\rm APD}(i,j)=f_{\rm APD}\int_0^{q_{\max}}\left[\left(\frac{\hbar^2 q_z^2\beta}{4m}\right)^{1/2}N(q_z)(e^{-\lambda_+^2}+e^{-\lambda_-^2})+e^{\lambda_-}\left(x_-+\frac{\sqrt{\pi}}{2}f_g(x_-)\right)\right]I_{ij}^2(q_z)\frac{1}{q_{\max}}dq_z, \quad \text{(A8)}$$

where

$$f_{\rm APD}=\frac{C_1^2 m^{3/2}q_{\max}}{\pi\rho C_s\hbar^3\beta^{1/2}}. \quad \text{(A9)}$$

Here, $\omega_q=C_s q_z$ in Eq. (A4) for acoustic phonons and $N(q_z)=1/[\exp(\hbar C_s q_z\beta)-1]$. C_s is the velocity of the longitudinal acoustic phonon.

For the *acoustic-phonon piezoelectric* effect:

$$P_{\rm APP}^p(i,j)=f_{\rm APP}^p\int_0^{q_{\max}}\left\{N^p(q_z)\left[e^{\lambda_+}f_g(x_+)\bar{K}_p^2(\theta_+)+e^{\lambda_-}f_g(x_-)\bar{K}_p^2(\theta_-)\right]+\sqrt{2}e^{\lambda_-}f_g(y_-)\bar{K}_p^2(\theta_-)I_{ij}^2(q_z)\frac{1}{q_{\max}}dq_z, \quad \text{(A10)}$$

where

$$f_{\rm APP}^p=\frac{e^2P^2(8\pi^3\beta m)^{1/2}}{\rho\epsilon_\infty^2\hbar}\frac{q_{\max}}{C_s^p} \quad \text{(A11)}$$

In Eq. (A10), y_- is defined as $[(\beta q_z^2\hbar^2/2m)^{1/2}x_-]^{1/2}$. The superscript and subscript p stands for polarization. Thus, $N^p(q_z)=1/[\exp(\hbar C_s^p q_z\beta)-1]$ and $\omega_q=C_s^p q_z$ in Eq. (A4). $\theta_\pm$ is defined as

$$\sin\theta_\pm=\frac{(2+\beta|\Delta E_\pm|)^{1/2}}{(2+\beta|\Delta E_\pm|+\hbar^2q_z^2\beta/2m)^{1/2}}. \quad \text{(A12)}$$

The $\bar{K}_p^2(\theta)$ is then given by

$$\bar{K}_L^2(\theta)=\frac{9}{8}\sin^4\theta\cos^2\theta, \quad \text{(A13)}$$

$$\bar{K}_{T_1}^2(\theta)+\bar{K}_{T_2}^2(\theta)=\frac{1}{8}(3\cos^2\theta-1)^2\sin^2\theta+\frac{1}{2}\cos^2\theta\sin^2\theta. \quad \text{(A14)}$$

In order to carry out the integral $\int_0^{q_{\max}}dq_z$ in Eqs. (A1), (A8), and (A10), we must first calculate $I_{ij}(q_z)$ defined in Eq. (A7). $I_{ij}(q_z)$ can be calculated numerically from $\psi_i(z)$ and $\psi_j(z)$, using fast Fourier transformation. However, here, we chose to calculate $I_{ij}(q_z)$ analytically from model $\psi_i(z)$ and $\psi_j(z)$. First, we model $\psi_i(z)$ as

$$\psi_i(z)=\alpha_i f(|z-z_i|)\cos\left(z\frac{\pi}{L_z}(i-1)+\theta_i\right), \quad \text{(A15)}$$

where L_z is the z direction length of the system, z_i is the central position of the localized wave function, θ_i is a phase shift, and α_i is a normalization factor. The state index i is counted from the lowest state of the system. $f(z)$ equals $e^{-2z/L_{\rm eff}}$ for $z<L_{\rm eff}$ and $e^{-2-(z-L_{\rm eff})\gamma}$ for $z>L_{\rm eff}$, where $L_{\rm eff}$ is the effective localization length of the state (shown in Fig. 1), $1/\gamma$ is the energy-dependent tail decay length of the state $[\gamma(E_i)]$ (shown in Fig. 2). By comparing to the directly calculated EMA wave functions, we found that Eq. (A15) models the wave function $\psi_i(z)$ well for all states. The factor $\cos[z(\pi/L_z)(i-1)+\theta_i]$ describes correctly the nodal structure of the state. In Eq. (A7), when we calculate $I_{ij}(q_z)$, assuming $j>i$, we let $\theta_i=0$ and adjust θ_j so that $\psi_i(z)$ and $\psi_j(z)$ are orthogonal. α_i, α_j are determined accordingly based on θ_i and θ_j. After that, $I_{ij}(q_z)$ can be carried out analytically as a function of z_i,z_j, θ_i,θ_j, and α_i,α_j.

After $I_{ij}(q_z)$ was obtained, integrals $\int_0^{q_{\max}}dq_z$ in Eqs. (A1) and (A8) and (A10) were performed numerically. Finally, $P(i,j)=P_{\rm OPP}(i,j)+P_{\rm APD}(i,j)+\Sigma_p P_{\rm APP}^p(i,j)$ was obtained for all pairs (i,j) in Fig. 2 for a given temperature. We

find that if $E_i > E_j$ by an amount larger than $\hbar\omega_0$, then $P_{\rm OPP}(i \rightarrow j)$ has the largest contribution of all P's at all temperatures. If E_i is not larger than E_j by $\hbar\omega_0$, then (i) at high temperature ($T > 100$ K), $P_{\rm OPP}$ has the largest contribution, (ii) at lower temperature ($T < 100$ K) and for small $E_j - E_i$ if $E_j > E_i$, $P_{\rm APP}$ has the largest contribution, followed by $P_{\rm APD}$ (a factor of 2–10 smaller than $P_{\rm APP}$).

The parameters used in Eqs. (A1),(A8), and (A10) are the following. Some of them are from calculations[13] and others from experimental results.[39] $P = (-0.32 - 0.45)/2$ C/m^2, $\hbar\omega_0 = (36+50)/2$ meV, ϵ_0(GaAs) = 12.85, ϵ_0(AlAs) = 10.06, ϵ_∞(GaAs) = 10.89, ϵ_∞(AlAs) = 8.16, C_1(el) = (11.38+10.56)/2 eV, C_1(hole) = (2.7+2.6)/2 eV, m(el) = (0.077+0.158)/2 electron mass, m(hole) = (0.416+0.439 + 0.079+0.157)/4 electron mass, $C_s^L = (36+44)/2$ meV/$q_{\rm max}$, $C_s^T = 0.58 C_s^L$, $q_{\rm max} = 2\pi/10.6826$ bohrs^{-1}. In the averages, the first number is the value of GaAs, the second number is for AlAs.

[1] A. Chomette, B. Deveaud, A. Regreny, and G. Bastard, Phys. Rev. Lett. **57**, 1464 (1986).

[2] A. Sasaki, M. Kasu, T. Yamamoto, and S. Noda, Jpn. J. Appl. Phys. **28**, L1249 (1989).

[3] L. Pavesi, E. Tuncel, B. Zimmermann, and F. K. Reinhart, Phys. Rev. B **39**, 7788 (1989).

[4] M. Kasu, T. Yamamoto, S. Noda, and A. Sasaki, Jpn. J. Appl. Phys. **29**, L1588 (1990).

[5] D. J. Arent, R. G. Alonso, G. S. Horner, D. Levi, M. Bode, A. Mascarenhas, J. M. Olson, X. Yin, M. C. DeLong, A. J. Spring Thorpe, A. Majeed, D. J. Mowbray, and M. S. Skolnick, Phys. Rev. B **49**, 11 173 (1994).

[6] K. A. Mäder, L.-W. Wang, and A. Zunger, Phys. Rev. Lett. **74**, 2555 (1995).

[7] K. A. Mäder, L.-W. Wang, and A. Zunger, J. Appl. Phys. **78**, 6639 (1995).

[8] V. Ambegaokar, B. I. Halperin, and J. S. Langer, Phys. Rev. B **4**, 2612 (1971).

[9] R. Tsu and G. Dohler, Phys. Rev. B **12**, 680 (1975).

[10] K. Hess, Appl. Phys. Lett. **35**, 484 (1979).

[11] D. Calecki, J. F. Palmier, and A. Chomette, J. Phys. C **17**, 5017 (1984).

[12] J. F. Palmier and A. Chomette, J. Phys. (Paris) **43**, 381 (1982).

[13] K. A. Mäder and A. Zunger, Phys. Rev. B **50**, 17 393 (1994).

[14] D. L. Rode, in *Transport Phenomena*, edited by R. K. Willardson and A. C. Beer, Semiconductors and Semimetals Vol. 10 (Academic, New York, 1975), p. 1.

[15] D. L. Rode, Phys. Rev. B **2**, 1012 (1970).

[16] C. Kittel, *Quantum Theory of Solids* (Wiley, New York, 1963).

[17] H. Stumpf, *Quantum Processes in Polar Semiconductors and Insulators* (Friedr. Vieweg & Sohn, Braunschweig, 1983), Pt. II.

[18] O. Madelung, *Introduction to Solid State Theory* (Springer-Verlag, Berlin, 1978).

[19] A. R. Hutson, J. Appl. Phys. Appl. Suppl. **32**, 2287 (1961).

[20] A. R. Hutson and D. L. White, J. Appl. Phys. **33**, 40 (1962).

[21] J. D. Zook, Phys. Rev. **136**, A869 (1964).

[22] In the analytical treatment of the acoustic-phonon effects, we have made a few approximations, which will result in less than a factor of 2 error. One approximation is $q/[\exp(\hbar C_s q\beta)-1] \approx q_z/[\exp(\hbar C_s q_z \beta)-1]$. The term involved is important only when $\hbar C_s q_{xy}\beta \ll 1$. Another approximation is $\int_0^{2\pi} d\theta (k^2+k'^2+q_z^2-2kk'\cos\theta)^{1/2} \approx 2\pi(k^2+k'^2+q_z^2)^{1/2}$. The term involved is important only when $k^2+k'^2 \gg 2kk'$. The last approximation concerns the averaging of K_h^2. It has been taken out from the integral as a constant, and replaced by an averaged value $\bar{K}_p^2(\theta)$, which is defined in Appendix A.

[23] When the initial state is taken at higher energies than the centroids, the largest resulting changes in Figs. 3 and 4 are confined to the first few picoseconds. One gets higher starting energy $E(t=0)$ and larger $\bar{d}^2$ ($t \sim$ picosecond). The $T=5$ K curves for both $E(t)$ and $\bar{d}^2(t)$ are slightly higher than the results shown in Figs. 3 and 4, but all the conclusions and analysis remain unchanged.

[24] A. J. Grant and E. A. Davis, Solid State Commun. **15**, 563 (1974).

[25] F. R. Shapiro and D. Adler, J. Non-Cryst. Solids **74**, 189 (1985); **77–78**, 139 (1985).

[26] We believe the formula in Ref. 11 for $W(i\vec{k}, j\vec{k}')$ is a factor of 2 too small compared to our Eq. (5), so the $D(T)$ values cited in the text include this correction.

[27] K. L. Ngai, A. K. Rajagopal, and S. Teitler, J. Chem. Phys. **88**, 5086 (1988).

[28] V. Halpern, J. Phys. D **25**, 1533 (1992).

[29] B. I. Shklovskii, H. Fritzsche, and S.D. Baranovskii, Phys. Rev. Lett. **62**, 2989 (1989).

[30] D. Monroe, Phys. Rev. Lett. **54**, 146 (1985).

[31] H. Scher and M. Lax, Phys. Rev. B **7**, 4491 (1973); H. Scher and E. W. Montroll, *ibid.* **12**, 2455 (1975); H. Scher, M. F. Shlesinger, and J. T. Bendler, Phys. Today **44** (1), 26 (1991).

[32] A. Blumen, J. Klafter, B. S. White, and G. Zumofen, Phys. Rev. Lett. **53**, 1301 (1984).

[33] P. Thomas and S. D. Baranovskii, J. Non-Cryst. Solids, **164–166**, 431 (1993).

[34] M. Grunewald and P. Thomas, Phys. Status Solidi B **94**, 125 (1979); M. Grunewald, P. Thomas, and D. Wurtz, *ibid.* **94**, K1 (1979).

[35] L. Banyai, in *Physique de Semiconducteurs*, edited by M. Hulin (Dunod, Paris, 1964), p. 417.

[36] M. H. Cohen, H. Fritzsche and S. R. Ovshinsky, Phys. Rev. Lett. **22**, 1065 (1969); E. A. Davis and N. F. Mott, Philos. Mag. **22**, 903 (1970).

[37] The experimental d-SL cited here is from Ref. 5, which has a long range correlation in its random layer sequences, thus is slightly different from our calculated d-SL, which does not have this correlation. However, for our purpose of rough estimates, these two systems are sufficiently similar as shown in Ref. 7.

[38] K. Uno, S. Noda, and A. Sasaki, J. Appl. Phys. **77**, 4693 (1995).

[39] S. Adachi, J. Appl. Phys. **58**, R1 (1985).